KEK Preprint 94-13
NWU-HEP 94-02
DPNU-94-18
INS-REP-1031
KOBE-HEP 94-04
OCU-HEP 94-02
PU-94-683
TIT-HEP 94-03
TUAT-HEP 94-02
May 1994
H

Measurement of the Photon Structure Function F_2^γ and Jet Production at TRISTAN

TOPAZ Collaboration

Submitted for publication.

NATIONAL LABORATORY FOR
HIGH ENERGY PHYSICS

National Laboratory for High Energy Physics, 1994

KEK Reports are available from:

Technical Information & Library
National Laboratory for High Energy Physics
1-1 Oho, Tsukuba-shi
Ibaraki-ken, 305
JAPAN

Phone: 0298-64-1171
Telex: 3652-534 (Domestic)
(0)3652-534 (International)
Fax: 0298-64-4604
Cable: KEK OHO
E-mail: LIBRARY@JPNKEKVX (Bitnet Address)
library@kekvax.kek.jp (Internet Address)

Measurement of the photon structure function F_2^γ and jet production at TRISTAN

(TOPAZ Collaboration)

K.Muramatsu[a], H.Hayashii[a], S.Noguchi[a], N.Fujiwara[a], K.Abe[c], T.Abe[d], I.Adachi[b], M.Aoki[d], M.Aoki[e], S.Awa[a], R.Belusevic[b], K.Emi[c], R.Enomoto[b], H.Fujii[b], K.Fujii[b], T.Fujii[f], J.Fujimoto[b], K.Fujita[g], B.Howell[h], N.Iida[b], H.Ikeda[b], R.Itoh[b], H.Iwasaki[b], M.Iwasaki[a], R.Kajikawa[d], K.Kaneyuki[e], S.Kato[i], S.Kawabata[b], H.Kichimi[b], M.Kobayashi[b], D.Koltick[h], I.Levine[h], S.Minami[e], K.Miyabayashi[d], A.Miyamoto[b], K.Nagai[j], T.Nagira[a], E.Nakano[d], K.Nakabayashi[d], O.Nitoh[c], F.Ochiai[k], Y.Ohnishi[d], H.Okuno[i], T.Okusawa[g], K.Shimozawa[d], T.Shinohara[c], A.Sugiyama[d], N.Sugiyama[e], S.Suzuki[d], K.Takahashi[c], T.Takahashi[g], M.Takemoto[a], T.Tanimori[e], T.Tauchi[b], F.Teramae[d], Y.Teramoto[g], N.Toomi[a], T.Toyama[d], T.Tsukamoto[b], S.Uno[b], T.Watanabe[e], Y.Watanabe[e], A.Yamaguchi[a], A.Yamamoto[b], and M.Yamauchi[b]

[a]:*Department of Physics, Nara Women's University, Nara 630, Japan*
[b]: *National Laboratory for High Energy Physics,KEK, Ibaraki-ken 305, Japan*
[c]:*Dept. of Applied Physics, Tokyo Univ. of Agriculture and Technology, Tokyo 184, Japan*
[d]:*Department of Physics, Nagoya University, Nagoya 464, Japan*
[e]:*Department of Physics, Tokyo Institute of Technology, Tokyo 152, Japan*
[f]:*Department of Physics, University of Tokyo, Tokyo 113, Japan*
[g]:*Department of Physics, Osaka City University, Osaka 558, Japan*
[h]:*Department of Physics, Purdue University, West Lafayette, IN 47907, USA*
[i]:*Institute for Nuclear Study, University of Tokyo, Tokyo 188, Japan*
[j]:*The Graduate School of Science and Technology, Kobe University, Kobe 657, Japan*
[k]:*Faculty of Liberal Arts, Tezukayama Gakuin University, Nara 631, Japan*

Abstract

We have measured the photon structure function F_2^γ in the reaction $e^+e^- \rightarrow e^+e^-$ hadrons for average Q^2 values from 5.1 to 338 GeV^2 by using data collected by the TOPAZ detector at TRISTAN. The data have been corrected for detector effects and are compared with theoretical expectations based on QCD. The structure function F_2^γ increases as $\ln Q^2$, as expected. A sample of events with one or two distinct jets has been identified in the final state. Although two-jet events can be explained solely by the point-like perturbative part, one-jet events require a significant hadron-like part in addition.

1 Introduction

A real photon has a dual nature. It interacts with matter as a point-like particle. The photon is also known to exhibit a hadronic nature behaving like a particle with an apparent substructure. In hadron production in the two-photon process,

$$e^+e^- \rightarrow e^+e^- + \text{hadrons} \tag{1}$$

studied under the single-tag condition (i.e. one of the final-state electron or positron is detected at a large angle and the other one is restricted to a small scattering angle), a quasi-real photon(γ) emitted from the undetected electron is probed by a high-Q^2 virtual photon(γ^*) from the tagged electron[1]. The process can be interpreted as a deep-inelastic electron scattering off a (quasi-)real photon target. The kinematics is illustrated in fig.1. The relevant underlying processes are shown in fig.2

Like the deep-inelastic electron-nucleon scattering, its cross section can be expressed in terms of two structure functions, $F_2^\gamma(x,Q^2)$ and $F_L^\gamma(x,Q^2)$ [2], as

$$\frac{d^2\sigma_{ee\rightarrow eeX}}{dxdy} = \frac{8\pi\alpha^2 E E_\gamma}{Q^4}\left[[1+(1-y)^2]F_2^\gamma(x,Q^2) - y^2 F_L^\gamma(x,Q^2)\right] f_{\gamma/e}(z)dz. \tag{2}$$

Here, $q^2 \equiv -Q^2 = -4E_{tag}E\sin^2(\theta_{tag}/2)$ is the square of the four-momentum transfer of the scattered electron and the scaling variables(x, y and z) are given by $x \equiv -q^2/2k\cdot q = Q^2/(Q^2+W^2)$, $y \equiv q\cdot k/p\cdot k = 1-(E_{tag}/E)\cos^2(\theta_{tag}/2)$ and $z = E_\gamma/E$, where q and k denote the 4-momenta of the probing(γ^*) and target(γ) photons, respectively. E_{tag} ,θ_{tag} are the energy and the scattering angle of the tagged electron, E is the beam energy, E_γ is the energy of the target photon and W is the invariant mass of the hadron system. The flux of the target photon $f_{\gamma/e}(z)$ is given by an equivalent photon approximation(EPA) [3]:

$$f_{\gamma/e}(z) = \frac{\alpha}{\pi}\frac{1}{z}\left\{\left[1+(1-z)^2\right]\ln\frac{2E(1-z)\sin(\theta_{max}/2)}{m_e z} - 1 + z\right\}, \tag{3}$$

where θ_{max} is the maximum scattering angle of the undetected electron. In most cases of this experiment, the second term in (2) is much smaller than the first one, since the average y^2 is less than 0.05 due to the tagging condition described below. We then neglected the second term and extracted F_2^γ from the measured cross section.

The first attempt to give a theoretical description of the photon structure function was given by E. Witten[4]. He suggested that the photon structure function is calculable perturbatively by quantum chromodynamics(QCD). However, it was realized that non-perturbative

effects are not negligible in the experimentally accessible (non-asymptotic) values of Q^2 and, more importantly, the hadronic non-perturbative components are essential to make the theory free from any unphysical singularities[5, 6]. Recently, interest in the structure of the photon has been reactivated. Several experimental collaborations have reported evidence for the production of high transverse-momentum(p_T) jets in both quasi-real $\gamma\gamma$ collisions at the e^+e^- colliders (TRISTAN[7, 8], LEP[9], PEP/PETRA[10]) and γp collisions at the ep collider HERA[11]. Indeed, we have shown that the rate of the high-p_T jet production in $\gamma\gamma$ collisions cannot be understood without including the effects of the photon structure (resolved photon process)[7]. Similar conclusions have also been obtained in γp collisions at HERA[11]. It is expected that a variety of processes which involve real photons could be understood by universal quark and gluon distributions in real photons[6]. Theoretical work on this subject started long ago[12].

So far, the F_2^γ structure function has been measured by several experimental collaborations at PETRA[13], PEP[14] and TRISTAN[15]. The available data are in the region $0.7 < Q^2 < 390$ GeV^2. However, the data are limited. Further measurements of the photon structure function are needed to improve our understanding of the nature of the real photon, which will play an important role in high-energy $\gamma\gamma$ and γp interactions.

In this paper, we present a measurement of the x-dependence of F_2^γ for three different Q^2 regions, corresponding to average Q^2 values of 5.1, 16, and 80 GeV^2. The range of x is extended down to 0.04 at $Q^2 = 5.1$GeV^2. In addition, the Q^2-dependence of F_2^γ for the intermediate x region ($0.3 < x < 0.8$) is measured over a wide-Q^2 region from 16 to 338 GeV^2. These ranges of Q^2 and x cover almost the entire region which has been reported in the previous experiments[13, 14, 15]. The measurement at the high-Q^2 region is important to check the basic Q^2 dependence of F_2^γ. The data at low-Q^2 regions are also important, since the theory needs some input distribution at low Q^2 to solve the inhomogeneous Altarelli-Parisi equations(IAPE)[5]. In particular, a measurement in low-x regions less than ~ 0.1 is interesting, since there the F_2^γ structure function is expected to be sensitive to its gluon contents of the photon[16]. Our results are compared with some of several parametrizations [15-20] obtained by solving IAPE as well as with that involving a different approach obtained by Field, Kapusta and Poggiolli(FKP)[22].

The results are also presented from a study of the final-state event topology in the single-tag two-photon events. Here, we directly searched for jets in the final state in order to study any possible difference in the event signature from the point-like and the hadron-like components of the photon[23].

2 Apparatus and Event Selection

The data used in this analysis were collected with the TOPAZ detector at the TRISTAN e^+e^- collider. Descriptions of the TOPAZ detector and its trigger system have been given in previous publications [23-25]. We briefly describe those features that are essential in this analysis. The momenta of charged particles are measured by a time-projection chamber (TPC) operated in a 1.0 T magnetic field. TPC covers the polar angular range $|\cos\theta| < 0.83$. Electrons and photons are detected by three different calorimeters: forward calorimeter (FCL), endcap calorimeter (ECL) and barrel calorimeter (BCL). These calorimeters cover 99.8% of 4π in total. FCL is a high-precision BGO calorimeter equipped with a silicon-strip detector[27]. It covers very low polar angular regions, $0.972 < |\cos\theta| < 0.9984 (= 3.2°)$. ECL is a lead-gas sampling device that covers the angular region $0.848 < |\cos\theta| < 0.978$. BCL consists of 4300 lead-glass Čerenkov counters. It covers the region $|\cos\theta| < 0.848$.

The tagging of scattered electrons was carried out by one of these calorimeters: FCL, ECL or BCL. In this paper we thus refer the events as FCL, ECL and BCL events, respectively. The ECL and BCL events were triggered by a requirement of large-energy deposition in these calorimeters. The FCL events were triggered mainly by the charged-track trigger[26]. The track trigger required at least two tracks with transverse momenta of $p_t > 0.3 - 0.7$ GeV and an opening angle $\phi > 45° - 70°$, depending on an experimental condition. This trigger-condition was essentially determined by the pre-track-trigger, which was based on the coincidence between hit information from the inner drift chamber and the TOF counters located outer-side of TPC.

Single-tagged two-photon events were further selected in an offline analysis. The selection criteria used for the ECL events are given below (those criteria for the FCL and BCL events are similar to those for the ECL events and the details are summarized in table 1):

(1) The energy of the tagged electron(or positron) must be greater than $0.3E_{beam}$. To ensure the best measured region of the detector, the polar angle is limited to be $0.89 \leq |\cos\theta_{tag}| \leq 0.96$.

(2) No additional clusters with an energy exceeding 0.2 E_{beam} can be observed anywhere in BCL and ECL(anti-tagging). This limits the maximum scattering angle of the undetected electron to be $|\cos\theta_{max}| = 0.98$.

(3) The charged multiplicity is three or more. The charged multiplicity includes only tracks which have transverse momenta greater than 0.15 GeV and have their closest distance to the beam interaction point less than 5 cm in the radial direction.

(4) The position of the event-vertex, reconstructed from all of the tracks, must be less than $\pm$ 5cm from the interaction point along the beam line.

(5) The visible mass of the hadron system (W_{vis}) must be greater than 1.0 GeV and less than E_{beam}, where both charged-tracks in TPC and neutral-clusters in BCL with an energy greater than 0.5GeV are used in the calculation of W_{vis}[†], and the pion mass is assumed for all charged particles.

(6) The vector sum of the transverse momenta ($\Sigma \mathbf{P}_t$), including that of the tagged electron, must be less than 0.3 E_{beam}.

(7) The total visible energy of the hadron system (E_{hadron}) should be less than $0.7E_{beam}$.

(8) The longitudinal momentum imbalance projected along the direction of the tagged electron $\{(\cos\theta_{tag}/|\cos\theta_{tag}|)\Sigma \mathbf{P}_z\}$ must exceed 0.6 E_{beam}.

(9) The sum of the absolute value of the momenta and cluster energies within a 0.4 radian cone with respect to the direction of the tagged electron, should be less than 0.7 GeV. This condition ensures the isolation of the tagged electron.

Criteria (6)-(9) are applied to suppress backgrounds from single-photon annihilation events.

A total of 2024 FCL, 285 ECL and 31 BCL events survived all of these selection criteria. The major source of background for the FCL events is beam-gas events. The beam-gas background was estimated from the number of events in the side-band of the event-vertex distribution along the beam axis. The beam-gas background was 21% for FCL events and was completely negligible for ECL and BCL events. The background due to $e^+e^- \to e^+e^-\tau^+\tau^-$ was calculated by a Monte-Carlo simulation using a program developed by Kuroda [28]. The program includes all order-α^4 QED diagrams, such as two-photon(multiperipheral) and bremsstrahlung processes. The contamination was estimated to be 4%(FCL), 8%(ECL) and 6%(BCL). Inelastic Compton scattering[23] is a major source of background for high-Q^2 regions. This background was estimated to be 2%(FCL), 7%(ECL), and 31%(BCL)[28]. The contamination of the single-photon annihilation events was estimated by the LUND Monte-Carlo program (version 6.3). The program, including electro-weak effects and an order-α initial state radiative correction, was found to reproduce both the background shape in E_{hadron} and the longitudinal momentum balance distributions well. The contamination was obtained to be 2%(FCL), 7%(ECL) and 10%(BCL). The background due to the processes $e^+e^- \to \tau^+\tau^-$,$\tau^+\tau^-\gamma$ and $\gamma\gamma \to e^+e^-, \mu^+\mu^-$ were found to be negligible[29].

After subtracting these backgrounds, 1452.7 ± 50.7(FCL), 221.5 ± 17.3(ECL) and 16.0 ± 6.1(BCL) events remain as the signal. The Q^2 values for the FCL events range from 3 to 30 GeV^2, while those for the ECL and BCL events cover the ranges 45-130 GeV^2 and 140-700 GeV^2, respectively. The integrated luminosity for the ECL and BCL events corresponds to 113.9 pb^{-1}, which were taken at the center-of-mass energy ($\sqrt{s}$) from 52 to 61.4GeV (the mean value is 57.9GeV). The FCL events were selected from 89.3 pb^{-1} experimental data at $\sqrt{s} = 58$GeV.

[†]In this analysis, we did not include the clusters in ECL in the calculation of W_{vis} and E_{hadron}, since the energy scale of ECL clusters less than a few GeV was not known well in the present level of caliburation.

3 Monte-Carlo Simulation

In order to compare our data with theory and to make an acceptance correction, Monte-Carlo events for the two-photon process (1) were generated according to the formula given by (1). We prepared two different Monte-Carlo samples in order to simulate the point-like and hadron-like parts in F_2^γ. The algorithm of the programs is essentially the same as the one used in previous experiments[8, 13]. For the point-like part of F_2^γ, the formula derived by F. Kapusta(FKP) were taken for the light quarks(u, d, s). The explicit formula are given in ref.[15]. Since the QCD scale parameter (Λ_{QCD}) in the formula is insensitive to F_2^γ, we fixed it at $\Lambda_{\rm QCD} = 0.2$ GeV. The cut-off parameter(p_T^0), which was introduced by the authors to separate point-like and hadron-like parts in F_2^γ, was treated as a free parameter. For the contribution of the charm quark to F_2^γ we used the lowest-order(QPM) expression [2],

$$\begin{aligned} F_2^c(x,Q^2) &= 3c_c^4\frac{\alpha}{\pi}x\left\{\Delta\left(8x(1-x)-1-4\frac{m_c^2}{Q^2}x(1-x)\right)\right. \\ &+ \left.\left(x^2+(1-x)^2+4\frac{m_c^2}{Q^2}x(1-3x)-8\frac{m_c^4}{Q^4}x^2\right)\ln\frac{1+\Delta}{1-\Delta}\right\}, \qquad (4) \\ &\text{with}\quad \Delta^2 = 1-\frac{4m_c^2x}{(1-x)Q^2}, \end{aligned}$$

in order to take the threshold effect of the c-quark into account. The c-quark mass was set to $m_c = 1.6$ GeV. The effect of the bottom quark was found to be negligible in this experiment.

For the hadron-like part of F_2^γ, we used the usual VMD(vector-meson dominance model) estimation derived from measurements of the pion structure function in the Drell-Yan process $\pi p \to \mu^+\mu^- X$ [2],

$$F_2^{\rm had} = 0.2\alpha(1-x). \qquad (5)$$

The final state of the hadronic system was simulated as $\gamma^*\gamma \to q\bar{q}$, but with different angular distributions for point-like and hadron-like parts, as described below. For the hadron-like part, we assumed the usual kinematics hold in the deep-inelastic lepton-nucleon scattering [23]; $p_{\rm struck} = q + xk$ and $p_{\rm rem.} = (1-x)k$, where $p_{\rm struck}$ and $p_{\rm rem}$ are the 4-momentum of the quark struck by the probing photon(γ^*) and that of the remnant part(jet), respectively (see fig.2a). These equations mean that the quark in the hadronic part of the photon is assumed to be on-mass shell. In the center of $\gamma^*\gamma$ system, this kinematics is equivalent to generate the struck quark along the γ^* direction and the remnant one along the

γ direction. In the laboratory(e^+e^- C.M.) system, the same kinematics results in a single jet at a large angle with respect to the beam axis and a remnant-jet in a small angle-region, as shown schematically in fig.2d. In the practical Monte-Carlo simulation, we introduced finite p_T with respect to the $\gamma^*\gamma$ axis in the form $d\sigma/dp_T^2 \propto e^{-3p_T^2}$; however, this does not change the basic feature of the final state.

For the point-like part, the final state is simulated as $\gamma^*\gamma \rightarrow q\bar{q}$ with the same angular distribution as in $\gamma\gamma$ using the formula given in ref.[30]. In contrast with the hadronic part, the point-like part gives rise to two jets, in many cases, at a large angle to the beam axis, as illustrated in fig.2e. In both models we took the usual quark masses: $m_u = m_d = 325$ MeV, $m_s = 500$ MeV and $m_c = 1.6$ GeV. The calculation of the cross sections and the event generation in the quark level were carried out by using the BASES/SPRING program[31]. The quarks were then fragmented into hadrons according to the LUND string-fragmentation scheme(version 6.3) [32]. The generated events were then passed through the TOPAZ detector simulation and the same analysis program as that used for the experimental data.

The Monte-Carlo simulations based on FKP(uds) + QPM(c)+ VMD with $p_T^0 = 0.5$ GeV predict 1442 ± 59(FCL), 188 ± 10(ECL), and 13.1 ± 0.5(BCL) events. These numbers agree well with the measured number of events. The distributions of the charged and neutral multiplicities, the transverse momentum spectra for charged and neutral particles with respect to the beam axis, Q^2 and W_{vis} for the FCL, ECL and BCL events were compared with the Monte-Carlo simulations after subtracting the background from the data on a bin-by-bin basis. We found that the Monte-Carlo simulations based on FKP(u,d,s)+ QPM(c)+ VMD can reproduce the data well in both the shape and the magnitude of the distribution.

4 Photon Structure Function(F_2^γ)

In order to compare our data with theoretical predictions directly, we have corrected the data for the detector acceptance and resolution, and extracted the structure function F_2^γ from the measured cross section. An acceptance correction(unfolding) was carried out with an unfolding technique developed by Blobel, which has been used in many groups for the measurement of F_2^γ [13, 14]. The details concerning the unfolding technique are described in the literature[33].

The results of F_2^γ at three bins of Q^2 are summarized in table 2. The first column in the table is the averaged value of Q^2 for each Q^2-bin. The interval of Q^2 is shown in the second column. The third column is the averaged value of x for a given x-interval specified in the fourth column. The fifth column gives the measured values of F_2^γ divided by the QED coupling constant(α). F_2^γ is measured down to $x = 0.043$ at $Q^2 = 5.1\text{GeV}^2$. We note that

the overall detection efficiency is sufficiently large and changes smoothly in the range of the x-interval shown in this table. In particular, the lower edge of the lowest x-bin is examined carefully by taking a region in which the efficiency is greater than about 20%. The first errors on F_2^γ/α are statistical and the second are systematic:

The systematic errors are obtained for each x-bin by taking a quadratic sum of the following sources.

(1) The systematic error due to the uncertainty of the trigger efficiency is $1 \sim 10\%$ for the FCL events, and is $\leq 1\%$ for the ECL events. Large uncertainties are found for FCL events at a large-x region, where the mass of the hadron system is small. It is caused by accidental hits(about 5% /counter/beam crossing) of the TOF counters, which are part of the logic for the charged-track trigger.

(2) The uncertainty due to background subtraction was 3%. The major source is the uncertainty of the background from the beam-gas interactions.

(3) The systematic error due to the cuts on the event selection was $3 \sim 4\%$. The major part of the uncertainty comes from an estimation of the annihilation events. The systematic error was estimated by changing the cut values applied to the total longitudinal-momentum distribution, where most of the annihilation events were eliminated.

(4) The overall uncertainty due to the luminosity measurements was 4 %.

(5) The difference in the final-state topology for the point-like and hadron-like(VMD) parts will cause a potentially large source of systematics. We estimated the systematics to be $2 \sim 13\%$ by changing the VMD contributions by $\pm 25\%$.

The total systematic errors for each x-bin were estimated to be $6.2 \sim 14\%$ by taking a quadratic sum of the individual errors.

The measured F_2^γ functions are compared with various theoretical predictions in figs.3a and 3b. The error bars in the data include both the statistical and systematic errors added in quadrature. In fig.3a, the data are compared with the sum of FKP(uds) + QPM(c) + hadron(VMD) predictions for three different values of p_T^0. The long-dashed, solid and short-dashed lines correspond to the cases $p_T^0 = 0.1$, 0.5, and 1.0 GeV, respectively. The contributions of hadron component(VMD) and the charm quark alone are shown by dotted and dot-dashed lines, respectively. The charm-quark contribution increases substantially in the higher Q^2 region [21]. Except for the lowest x-bin at $Q^2 = 16$ GeV^2, the data agree with the FKP predictions if p_T^0 is taken to be less than 1.0 GeV.

In fig.3b, the results are compared with three different leading-log order predictions given by Drees-Grassie(DG)[17], Levy-Abramowicz-Charchula(LAC)[18] and Gück-Reya-Vogt (GRV)[19]. Although all of these predictions are based on the inhomogeneous Q^2-evolution equations(IAPE) given by QCD, different choices are made in the treatment of the input-distribution. The short-dashed, long-dashed and solid lines correspond to DG, LAC1[¶] and GRV, respectively. Although higher order predictions are also available for GRV, they are not shown here, since they are similar to that of the leading-order GRV predictions in the kinematical region of this experiment. The data at $Q^2 = 80$ GeV^2 agree with these predictions, but the data at $Q^2 = 16$ and 5.1 GeV^2 show some excess over these predictions for the x region less than ~ 0.2.

One basic feature of the photon structure function is the Q^2-dependence. In order to study this dependence, we extracted the average values of F_2^γ/α in the intermediate x region (0.3 - 0.8) for the averaged Q^2 from 16 to 338 GeV^2:

$$\begin{aligned} < F_2^\gamma/\alpha > &= 0.47 \pm 0.08 \ \ (0.38 \pm 0.08) \ \text{ at } \ Q^2 = 16 \text{ GeV}^2 , \\ < F_2^\gamma/\alpha > &= 0.70 \pm 0.15 \ \ (0.49 \pm 0.15) \ \text{ at } \ Q^2 = 80 \text{ GeV}^2 \\ \text{and} \quad < F_2^\gamma/\alpha > &= 1.07 \pm 0.37 \ \ (0.72 \pm 0.37) \ \text{ at } \ Q^2 = 338 \text{ GeV}^2 . \end{aligned}$$

The quoted errors are the quadratic sum of the statistical and systematic errors. The numbers given in the parenthesis are the results for light quarks (u, d, s) alone. These values were obtained by subtracting the charm-quark contribution from the data by using the lowest-order formula given in eq.(4). We show these subtracted values here, since some results in the previous experiments are presented in this way[8, 34]. It should however be noted that this subtraction introduces theoretical uncertainties caused by the uncertainty of the c-quark mass and the higher-order corrections to the c-quark contents of F_2^γ[21]. These uncertainties are not included in the errors of the subtracted results.

The data at the highest Q^2 region correspond to the BCL events, which cover the Q^2-range from 140 to 700 GeV^2. For this region, non-negligible contributions from the F_L^γ term are found. This contribution was calculated from the QPM expression [2] to be 10%, and was subtracted from the data. The subtracted results are plotted in fig.4 together with the previous measurements [34]. Also plotted in the figure are the sum of the FKP(uds) and VMD predictions for various values of p_T^0. The data show a clear increase of F_2^γ as Q^2 rises and its slope is consistent with the $\ln Q^2$-dependence which is expected from QPM and QCD.

[¶]We used the formula given in (4) for the c-quark contribution to obtain the prediction of LAC1. The shape is thus different from those given in the original paper[18].

5 Jet Analysis

As mentioned in Sec. 3 and also emphasized in ref.[23], the point-like and hadron-like parts of the photon should result in different final-state topologies. To test this expectation, we studied jet production in the deep-inelastic $e\gamma$ scattering by using the sample of the FCL events ($3.0 < Q^2 < 30$GeV^2). Jets in the final state were reconstructed with a jet-cone algorithm in azimuth (ϕ) and pseudorapidity (η) space[35]. The pseudorapidity(η) is defined as $\eta = -\ln\tan(\theta/2)$, where θ is the polar angle of the particles with respect to the beam axis. The detailed procedure of the jet-clustering algorithm is described in ref.[7]. The cone radius, $R = \sqrt{(\triangle\phi^2 + \triangle\eta^2)}$, was chosen to be 1 unit. All charged tracks whose transverse momenta greater than 0.15 GeV and neutral particles whose energies greater than 0.5 GeV were used in the jet-search. The polar-angles for the charged tracks and neutral particles were limited to $|\cos\theta| < 0.85$. The activity due to the tagged electron was excluded in the jet-search. We accepted those clusters as a jet if its transverse momentum was greater than 2.0 GeV. To ensure that jets were well contained within the detector, the jet axis was restricted to be $|\eta_J| \leq 0.7$.

With the above criteria, 718(49%), 646(45%) and 87(6%) events belonging to the zero- , one- and two-jet categories were found after subtracting the background. The zero-jet events are caused by cuts applied to jet-transverse momentum (jet-p_T) and η_J. Lego-plots of the transverse momentum distribution for typical one-jet and two-jet events are shown in figs.5a and b, respectively. In both figures, clearly isolated clusters in addition to the activity of the tagged electron are observed. The figure of the one-jet sample demonstrates how the transverse momentum is balanced between the tagged electron and the hadronic jet.

It is expected that the hadron-like part should not give two high-p_T jets, at least in leading-order in QCD. The two-jet sample should therefore be described by the point-like part alone. This parton level expectation should hold in the hadron level and also after the detector simulation. Indeed, the Monte-Carlo simulation for the point-like part (the sum of FKP(uds) and QPM(c)) predicts the fraction of jet-multiplicity to be 50%, 42% and 8% for the zero-, one- and two-jet categories, while a simulation for the hadron-like part results in 78%(zero-jet), 22%(one-jet) and 0%(two-jet). As expected, the two-jet events appear only in the point-like part. The jet-transverse momentum distribution is compared with the Monte-Carlo predictions in figs.6a and 6b for two-jet and one-jet events, respectively. The histogram given in fig.6a is a prediction of the point-like part, where the total number is normalized to that of the two-jet events observed in the data. The shape of the jet-p_T distribution for the two-jet sample is well reproduced with the point-like part alone. On the contrary, the jet-p_T distribution for the one-jet sample cannot be explained by the point-like part alone, as shown by the solid histogram in fig.6b. In this histogram the normalization of the point-like part is also fixed to that of the two-jet sample. The prediction is thus insensitive to special models

assumed for the point-like part of F_2^γ. We can clearly observe an excess over the point-like part in the region of jet-p_T less than 3 GeV. This excess can be explained by adding the hadron-like part, as shown by the dashed line in fig.6b. A fit of the data to a superposition of both Monte-Carlo distributions leads a best-value for the fraction of the hadron-like part to be $44 \pm 8\%$. The error includes only the statistical uncertainty. The result is consistent with the value (37%) when the FKP formula is used for the point-like part ($p_T^0 = 0.5$ GeV) and the VMD formula for the hadron-like part.

6 Summary

We have measured the photon structure function $F_2^\gamma(x, Q^2)$ for a wide-Q^2 region. The structure function increases as $\ln Q^2$, as expected by QPM and QCD. The overall behaviour of the x dependence of the F_2^γ is consistent with the various predictions based on QCD, but some deviations are observed in the region of x less than ~ 0.2 at average Q^2 values of 16 and 5.1 GeV^2.

The jet production in deep-inelastic $e\gamma$ scattering was studied for the first time with a jet-cone algorithm. The two-jet events are consistent with the expectation from the point-like perturbative part. While an excess over the point-like component is observed in the one-jet sample, which is direct experimental evidence for the existance of the hadron-like component in deep-inelastic $e\gamma$ scattering. The fraction of the hadron-like part in the region $3.0 < Q^2 < 30$GeV^2 was found to be $44 \pm 8\%$.

Acknowledgement

We thank Dr. M.T. Ronan for providing us the Blobel's unfolding program, which has been used in the TPC/2γ collaboration. We acknowledge Drs. M. Drees, E. Laenen and K. Hagiwara for valuable discussions about the analysis of F_2^γ and jet production. We thank the TRISTAN accelerator staff for the excellent operation of the storage ring. We also acknowledge the help of the managements and technical staff of KEK and all outside institutions collaborating in TOPAZ.

References

[1] S.J. Brodsky, T. Kinoshita and H. Terazawa, *Phys. Rev. Lett.*, **27**(1971)280.

[2] Ch. Berger and W. Wagner, *Phys. Rep.*, **146**(1987)1.

[3] V.M. Budnev *et al.*, *Phys. Rep.*, **15**(1975)181.

[4] E. Witten, *Nucl. Phys.*, **B120**(1977)189.

[5] M. Glück,K. Grassie, and E. Reya, *Phys. Rev.*, **D30**(1984)1447.

[6] M. Drees and R.M. Godbole, *Nucl. Phys.*, **B339**(1990)355.

[7] TOPAZ Collab., H. Hayashii *et al.*, *Phys. Lett.*, **B314**(1993)149.

[8] AMY Collab., R. Tanaka *et al.*, *Phys. Lett.*, **B277**(1992)215.

[9] ALEPH Collab., D. Buskulic *et al.*, *Phys. Lett.*, **B313**(1993)509.

[10] PLUTO Collab., Ch. Berger *et al.*, *Z. Phys.*, **C33**(1987)351;
CELLO Collab., H.J. Behrend *et al.*, *Z. Phys.*, **C51**(1991)365;
TPC/Two-Gamma Collab., H. Aihara *et al.*, *Phys. Rev.*, **D41**(1991)2667.

[11] H1 Collab., T. Ahmed *et al.*, *Phys. Lett.*, **B297**(1992)205;
ZEUS Collab., M. Derrick *et al.*, *Phys. Lett.*, **B297**(1992)404.

[12] G.H.Llewellyn-Smith, *Phys. Lett.*, **79B**(1978)83; S.J. Brodsky,T.A. DeGrand, J.F. Gunion and S. Weis, *Phys. Rev. Lett.*, **41**(1978)672, and *Phys. Rev.*, **D19**(1979)1418; K. Kajantie and R. Raitio, *Nucl. Phys.*, **B159**(1979)528; H. Terazawa, J. Phy. Soc. of Japan **47**(1979)355.

[13] PLUTO Collab., Ch. Berger *et al.*, *Z. Phys.*, **C26**(1984)353, *Phys. Lett.*, **B142**(1984)111, *Phys. Lett.*, **B149**(1984)421, and *Nucl. Phys.*, **B281**(1987)365;
TASSO Collab., M. Althoff *et al.*, *Z. Phys.*, **C31**(1986)527;
JADE Collab., W. Bartel *et al.*, *Z. Phys.*, **C24**(1984)231;
CELLO Collab., H.J. Behrend *et al.*, *Phys. Lett.*, **B126**(1983)391.

[14] TPC/2γ Collab., H. Aihara *et al.*, *Z. Phys.*, **C34**(1987)1, *Phys. Rev. Lett.*, **58**(1987)97, D. Bintiger *et al.*, *Phys. Rev. Lett.*, **54**(1985)763.

[15] AMY Collab., T. Sasaki *et al.*, *Phys. Lett.*, **B252**(1990)491.

[16] I. Watanabe KEK-preprint TH-387(1994).

[17] M. Drees and K. Grassie, *Z. Phys.*, **C28**(1985)451.

[18] H. Abramowicz, K. Charchula and A. Levy, *Phys. Lett.*, **B269**(1991)458.

[19] M.Glück, E. Reya and A. Vogt, *Phys. Rev.*, **D46**(1993)1973.

[20] L.E. Gordon and J.K. Storrow, *Z. Phys.*, **C56**(1992)307.

[21] E. Laenen, S. Riemersma, J. Smith, W.L. van Neerven, Fermilab preprint, FERMILAB-Pub-93/240-T

[22] J.H. Field, F. Kapusta, and L. Poggioli, *Phys. Lett.*, **B181**(1986)362, *Z. Phys.*, **C36**(1987)121; F. Kapusta, *Z. Phys.*, **C42**(1989)225.

[23] C. Peterson, P.M. Zerwas and T.F. Walsh, *Nucl. Phys.*, **B229**(1983)301 and private communication with M. Drees.

[24] TOPAZ Collab., I. Adachi *et al.*, *Phys. Rev. Lett.*, **60**(1988)97.

[25] TPC: T. Kamae *et al.*, *Nucl. Instr. and Meth.*, **A252**(1986)423; A. Shirahashi *et al.*, *IEEE Trans. on Nucl. Sci.* **NS-35**(1988) 414.
TOF: T. Kishida *et al.*, *Nucl. Instr. and Meth.*, **A254**(1987)367.
BCL: S. Kawabata *et al.*, *Nucl. Instr. and Meth.*, **A270**(1988)11.
ECL: K. Fujii *et al.*, *Nucl. Instr. and Meth.*, **A236**(1985)55; J. Fujimoto *et al.*, *Nucl. Instr. and Meth.*, **A256**(1987)449.

[26] R. Enomoto *et al.*, *Nucl. Instr. and Meth.*, **A269**(1988)507, *IEEE Trans. on Nucl. Sci.* **NS-35**(1988)419, T. Tsukamoto *et al.*, *Nucl. Instr. and Meth.*, **A297**(1990)148.

[27] FCL: H. Hayashii *et al.*, *Nucl. Instr. and Meth.*, **A316**(1992)202.

[28] M. Kuroda, Meiji Gakuin University(Tokyo) Rep. J.424(1988)27.

[29] TOPAZ Collab., B. Howell *et al.*, *Phys. Lett.*, **B291**(1992)206; H. Hayashii *et al.*, *Phys. Lett.*, **B279**(1992)422.

[30] S. Brodsky, T. Kinoshita and H. Terazawa, *Phys. Rev.*, **D41**(1971)1532.

[31] S. Kawabata, *Comput. Phys. Commun.* **41**(1986) 127.

[32] T. Sjöstrand, *Comput. Phys. Commun.* **39**(1986) 347 and T. Sjöstrand and M. Bengtsson, *Comput. Phys. Commun.* **43**(1987) 367. The sysmetric LUND fragmentation function without parton-shower were used with the default(version 6.3) parameters of $\sigma_q = 0.4$ GeV, $a = 1.0$, and $b = 0.7$ GeV^{-2}.

[33] V. Blobel, DESY Report 84-118(1984), A. Baecker, Proc. Intern. Workshop on $\gamma\gamma$ Collisions, Lake Tahoe, ed. R.L. Lander(World Scientific, 1984).

[34] See fig.6.41 in p123 in the ref.[2] and see also references therein. AMY data are taken from ref.[15].

[35] S.D. Ellis, Z. Kunszt and D.E. Soper, *Phys. Rev.*, **D40**(1989)2188.

Tagging device		FCL	ECL	BCL
$e^{\pm}$ tag	E_{tag}/E_{beam}	$\geq$0.3	$\geq$0.3	$\geq$0.3
	$\|\cos\theta_{tag}\|$	0.98–0.998	0.89–0.96	$\leq$0.8
$e^{\mp}$ anti-tag	$E_{cluster}/E_{beam}$	$\leq$0.2	$\leq$0.2	$\leq$0.2
	$\|\cos\theta_{anti-tag}\|$	$\leq$0.998	$\leq$0.98	$\leq$0.98
Hadron selection	$N_{charged}$	$\geq$3	$\geq$3	$\geq$3
	$\|V_Z\|$ (cm)	$\leq$ 5.	$\leq$ 5.	$\leq$ 5.
	W_{vis} (GeV)	1. – 29.	1. – 29.	2. – 29.
Background rejection	$\sum \mathbf{P_t}/E_{beam}$	$\leq$ 0.3	$\leq$ 0.3	$\leq$ 0.3
	E_{hadron}/E_{beam}	$\leq$ 0.6	$\leq$ 0.7	$\leq$ 1.0
	$(\sum \mathbf{P}_z)\frac{\cos\theta_{tag}}{\|\cos\theta_{tag}\|}/E_{beam}$	$\geq$ 0.6	$\geq$ 0.6	$\geq$ 0.4
	$\sum\|P^{\theta\leq\theta_0}\|$ (GeV)	not used	$\leq$ 0.7	$\leq$ 2.
	θ_0 (rad)	not used	0.4	0.8

Table 1: Selection criteria for the events $e^+e^- \rightarrow e^+e^-$ + hadrons tagged by the forward(FCL), end-cap(ECL) and barrel(BCL) calorimeters.

$< Q^2 >$ $(\mathrm{GeV})^2$	Q^2 $(\mathrm{GeV})^2$	$< x >$	x	F_2^γ/α
5.1	3 – 10	0.043	0.010 – 0.076	0.33 $\pm$ 0.02 $\pm$ 0.05
		0.138	0.076 – 0.20	0.29 $\pm$ 0.03 $\pm$ 0.03
16	10 – 30	0.085	0.02 – 0.15	0.60 $\pm$ 0.08 $\pm$ 0.06
		0.24	0.15 – 0.33	0.56 $\pm$ 0.09 $\pm$ 0.04
		0.555	0.33 – 0.78	0.46 $\pm$ 0.15 $\pm$ 0.06
80	45 – 130	0.19	0.06 – 0.32	0.68 $\pm$ 0.26 $\pm$ 0.05
		0.455	0.32 – 0.59	0.83 $\pm$ 0.22 $\pm$ 0.05
		0.785	0.59 – 0.98	0.53 $\pm$ 0.21 $\pm$ 0.05

Table 2: Measured values of the photon structure function F_2^γ/α at $< Q^2 >= 5.1$, 16 and 80 GeV^2. The first errors on F_2^γ/α are statistical and the second systematic.

Figure Captions

Fig.1: Deep inelastic electron photon scattering in e^+e^- reactions.

Fig.2: Different contributions to the photon structure function: (a) contribution of the hadronic part of the photon; (b) quark-pair production; (c) QCD corrections to (b). The final-state event topology expected from each contribution: (d) the event configulation of (a); (e) that of (b) and (c). In (d) and (e) the hadronic jets are indicated by big arrows.

Fig.3: Comparison of the F_2^γ structure function with theoretical predictions. The error bars in the data include the statistical and systematic errors: (a) The sum of the FKP(uds) + QPM(c) + hadron(VMD) predictions for three different values of $p_T^0 = 0.1$(long-dashed),0.5(solid),and 1.0 GeV(short-dashed). The dotted and dot-dashed lines are the contributions form the hadron-like(VMD) part and the charm quark alone, respectively.; (b) The leading order QCD predictions of GRV(solid), DG(short-dashed) and LAC1(long-dashed). For the charm quark, the formula (4) is used to obtain the GRV and LAC1 predictions.

Fig.4: Q^2-dependence of the F_2^γ structure function averaged over the intermediate x region between 0.3 and 0.8 along with the results from the previous experiments. The charm-quark contribution has been subtracted from the data. The theoretical expectations for the FKP + VMD predictions are shown for $p_T^0 = 0.1$, 0.5 and 1 GeV. The long-dashed line is the contribution of VMD alone.

Fig.5: Lego plots of typical one-jet(a) and two-jet events(b) in the single-tag two-photon events. The transverse momenta are shown in the plane of the pseudorapidity (η) and azimuthal angle (ϕ).

Fig.6: Transverse momentum of jets for the two-jet (a) and one-jet (b) events in the single-tag two-photon sample($3.0 < Q^2 < 30$ GeV^2); (a): The solid histogram shows the Monte-Carlo prediction of the point-like part alone. The Monte-Carlo sample has been normalized to the total number of the two-jet events measured in the data. (b): The solid histogram is the prediction of the point-like part, where the normalization is fixed in the two-jet events. The dashed line is the sum of hadron-like and point-like parts for the case of the best mixture of two parts. The contribution of the hadronic part alone is shown by the dotted histogram.

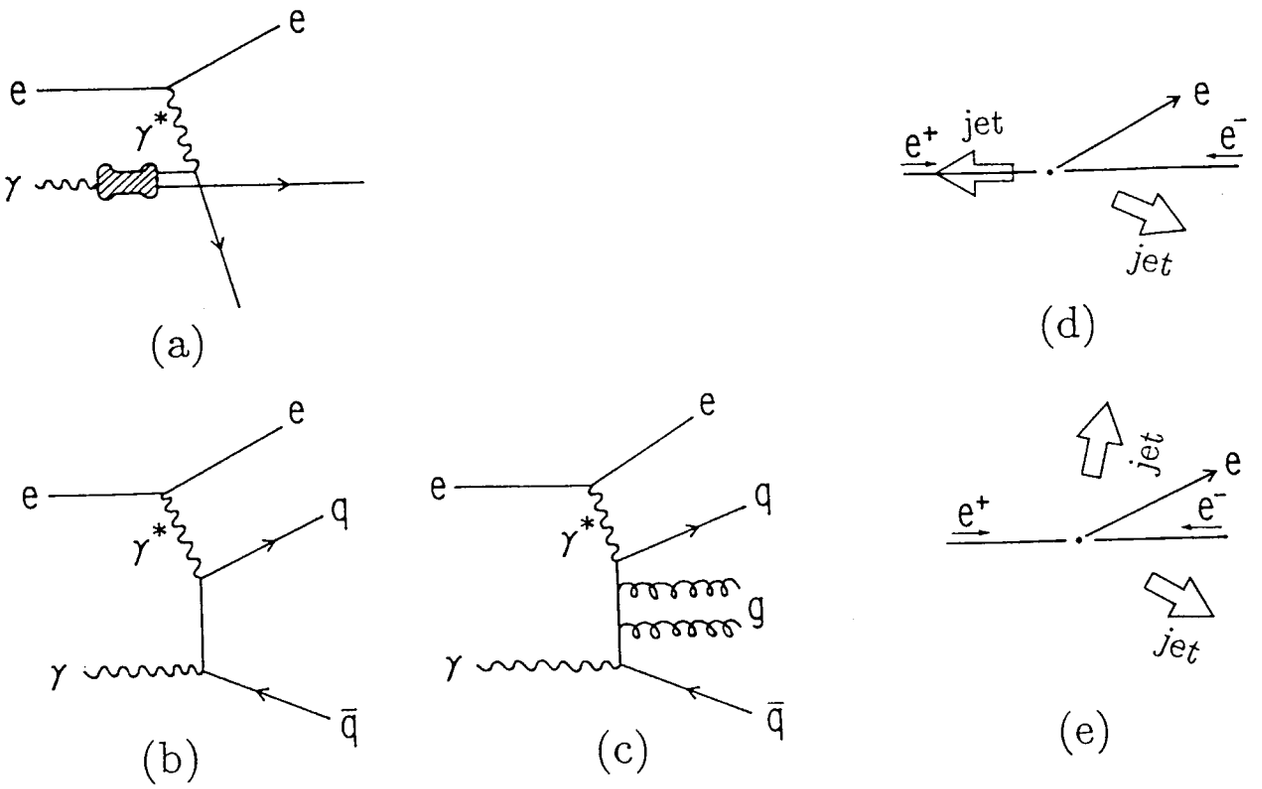
e
e
γ*
γ
(a)
e
e
γ*
q
γ
q̄
(b)
e
e
γ*
q
g
γ
q̄
(c)
e⁺
jet
e
e⁻
jet
(d)
jet
e
e⁺
e⁻
jet
(e)

Fig.2

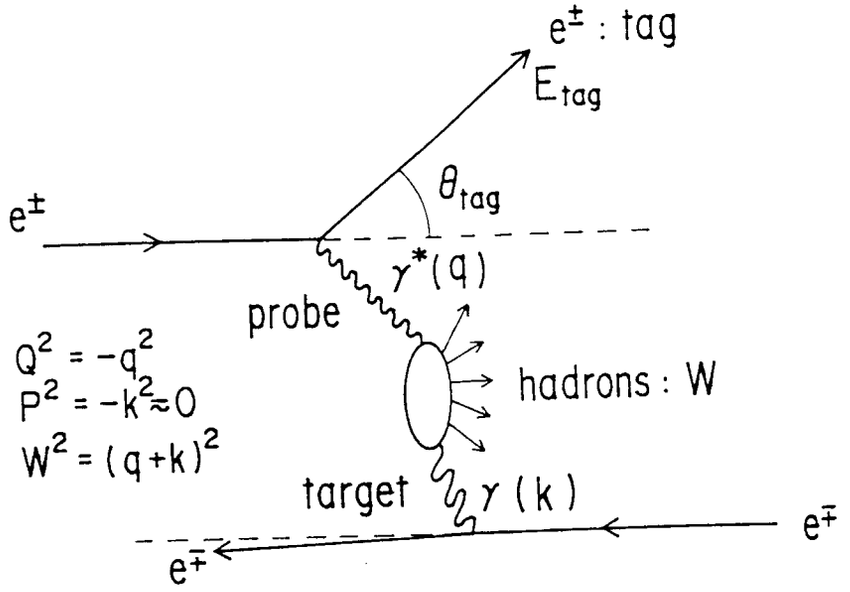
e± : tag
E_tag
θ_tag
e±
γ*(q)
probe
Q² = −q²
P² = −k² ≈ 0
W² = (q+k)²
hadrons : W
target
γ (k)
e∓
e∓

Fig. 1

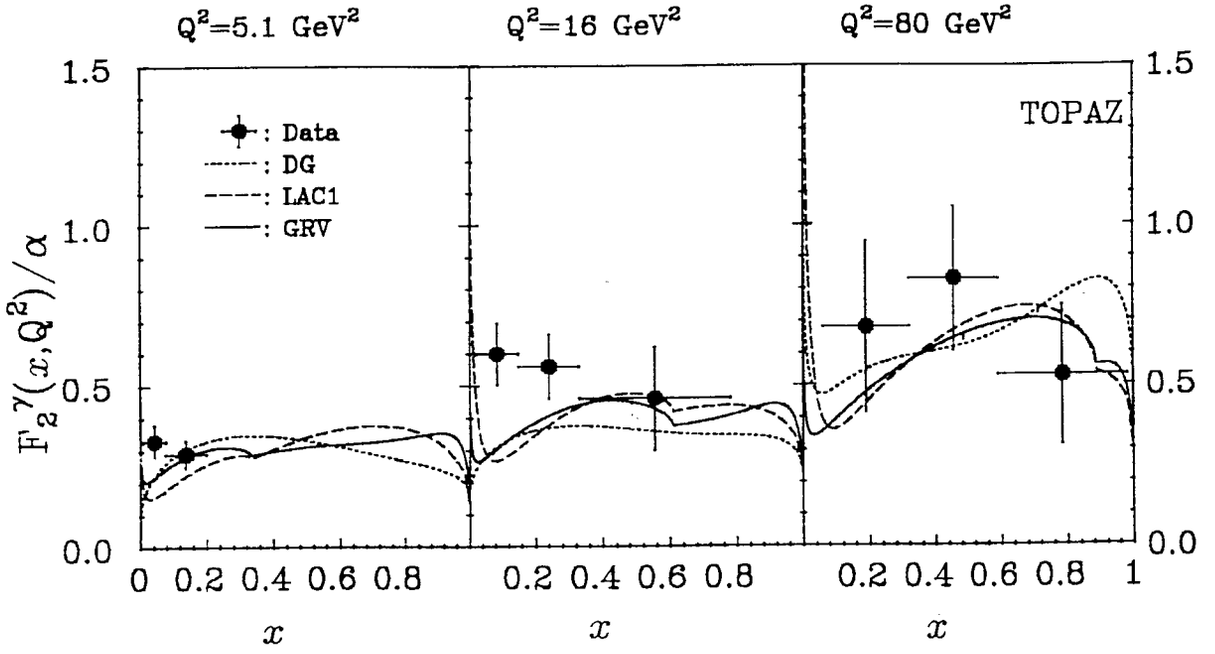
Q^2=5.1 GeV^2
Q^2=16 GeV^2
Q^2=80 GeV^2
TOPAZ
: Data
: DG
: LAC1
: GRV
$F_2^\gamma(x,Q^2)/\alpha$
x

Fig.3b

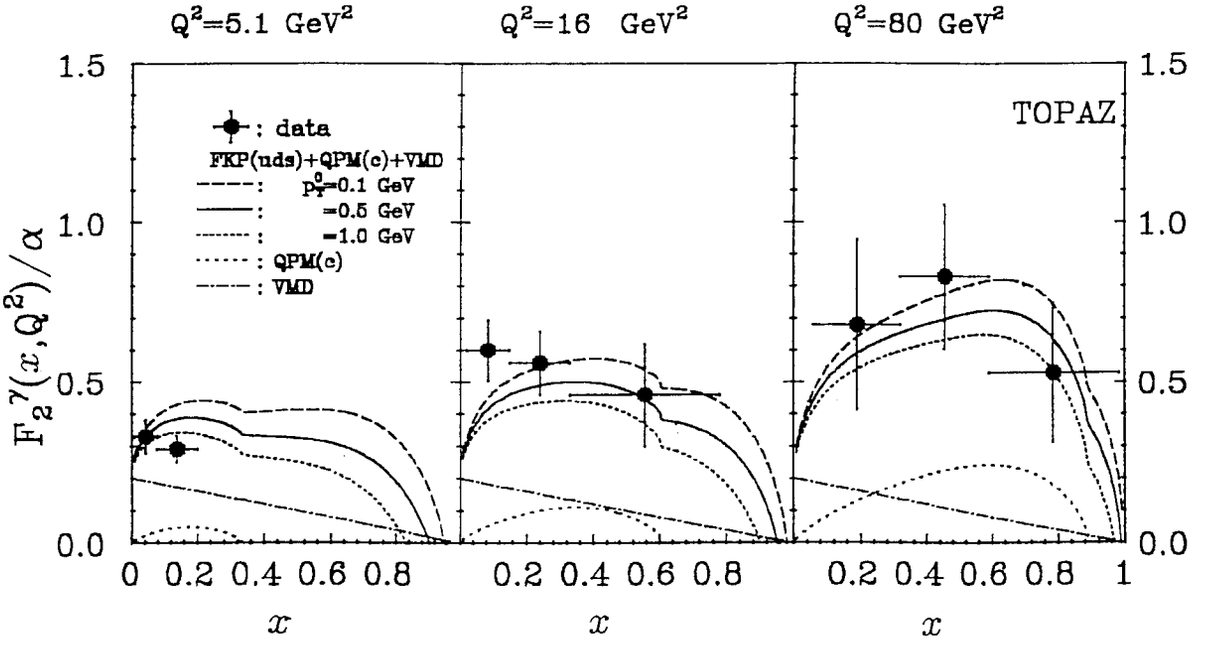
Q^2=5.1 GeV^2
Q^2=16 GeV^2
Q^2=80 GeV^2
TOPAZ
: data
FKP(uds)+QPM(c)+VMD
: p_T^0=0.1 GeV
: =0.5 GeV
: =1.0 GeV
: QPM(c)
: VMD
$F_2^\gamma(x,Q^2)/\alpha$
x

Fig.3a

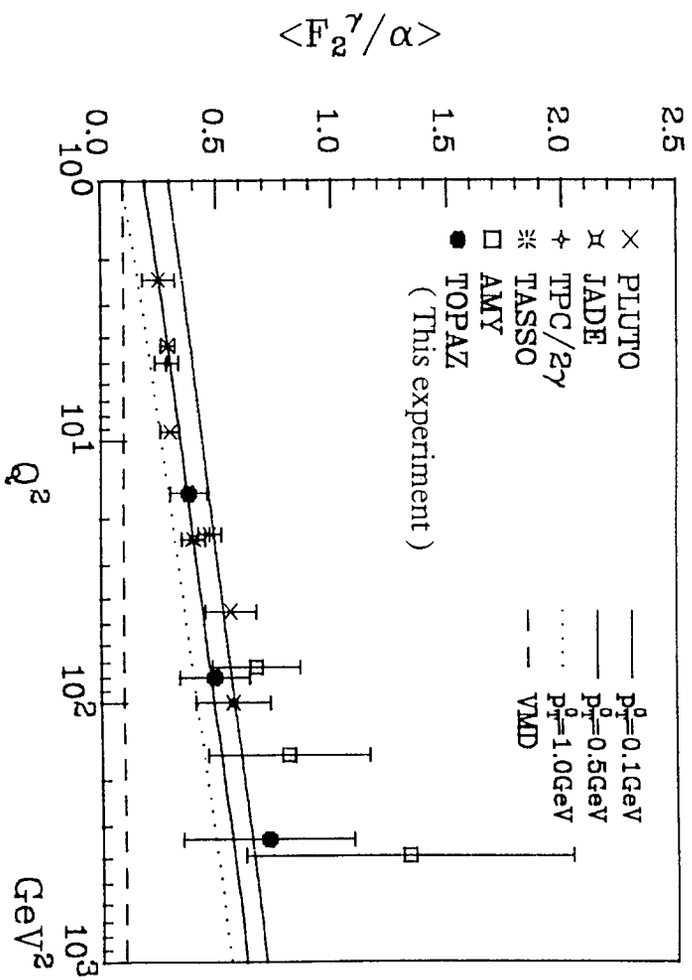
$<F_2^\gamma/\alpha>$
0.0
0.5
1.0
1.5
2.0
2.5
10^0
10^1
10^2
10^3
Q^2
GeV^2
PLUTO
JADE
TPC/2γ
TASSO
AMY
TOPAZ
(This experiment)
p_T^0=0.1GeV
p_T^0=0.5GeV
p_T^0=1.0GeV
VMD

Fig. 4

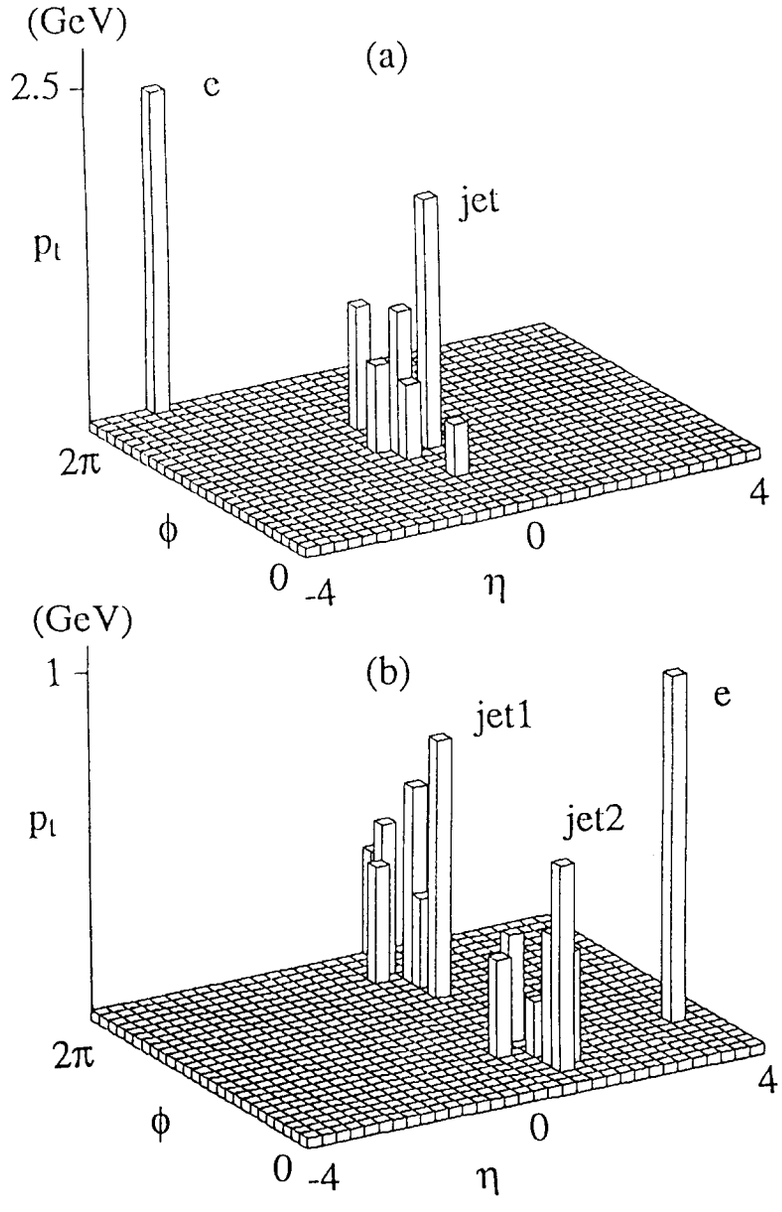
(GeV)
(a)
2.5
c
jet
p_t
2π
φ
0
-4
η
4
(GeV)
(b)
1
jet1
e
p_t
jet2
2π
φ
0
-4
η
4

Fig. 5

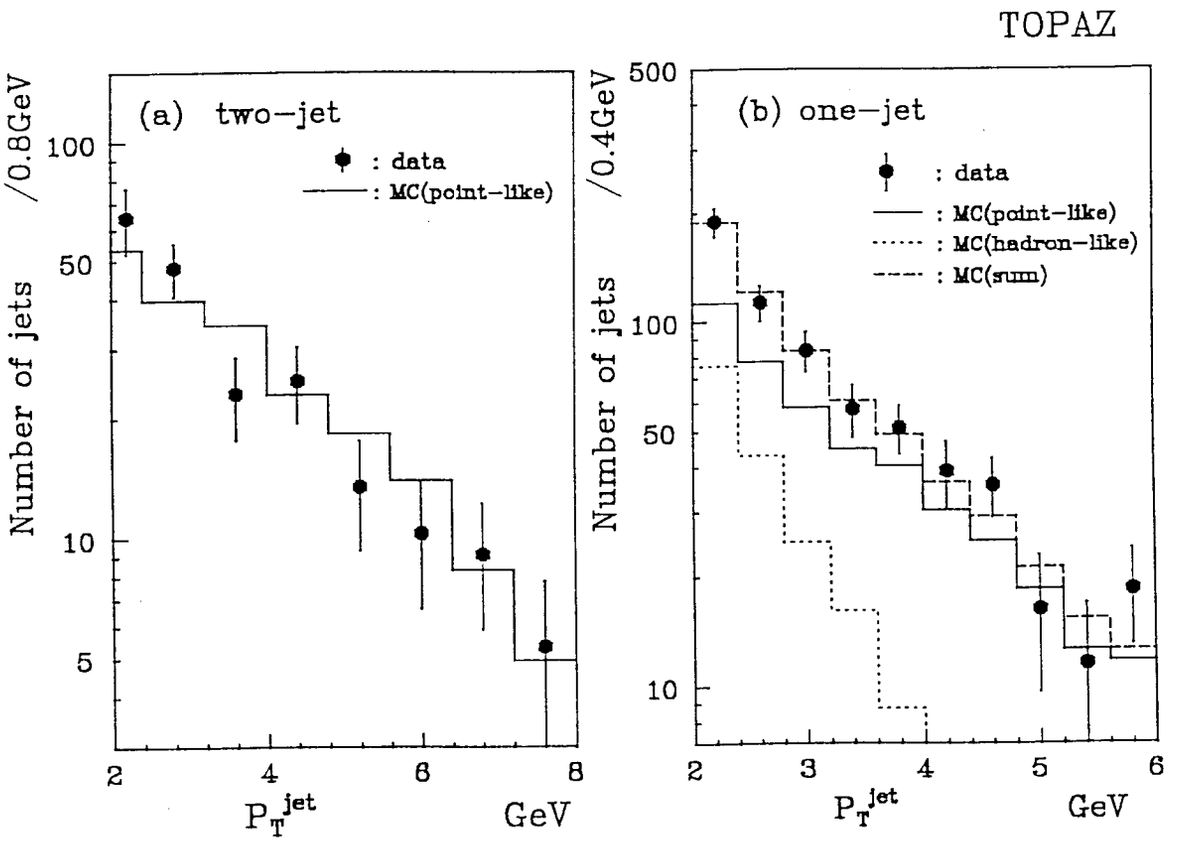
TOPAZ
(a) two-jet
: data
: MC(point-like)
Number of jets /0.8GeV
100
50
10
5
2
4
6
8
P_T^{jet}
GeV
(b) one-jet
: data
: MC(point-like)
: MC(hadron-like)
: MC(sum)
Number of jets /0.4GeV
500
100
50
10
2
3
4
5
6
P_T^{jet}
GeV

Fig.6